High Spectral Efficiency PM-128QAM Comb-Based Superchannel Transmission Enabled by a Single Shared Optical Pilot Tone

Mikael Mazur, *Student Member, OSA*, Abel Lorences-Riesgo, Jochen Schröder, *Member, IEEE, Member, OSA*, Peter A. Andrekson, *Fellow, IEEE, Fellow, OSA*, and Magnus Karlsson, *Senior Member, IEEE, Fellow, OSA*

(Highly-Scored Paper)

***Abstract*—We exploit the coherence of frequency combs for high spectral efficiency superchannel transmission via effective sharing of a single pilot tone. By phase-locking the receiver comb to the transmitted pilot tone, carrier offsets are suppressed while both the overhead and complexity associated with the pilot tone are reduced. We form a 55 carrier superchannel using a 25-GHz spaced electro-optic frequency comb seeded by a 100-kHz linewidth laser. At a pilot tone overhead of <2%, the reduction in carrier offsets is shown to facilitate blind DSP-based carrier recovery of all 54 × 24 Gbaud PM-128QAM data channels. The resulting superchannel spectral efficiency is 10.3 bits/s/Hz assuming a 28% overhead for forward error correction. Our results show the potential for optical pilot tones to reduce both overhead and complexity in systems using comb-based superchannels together with high-order modulation formats.**

***Index Terms*—Analog optical signal processing, coherent communications, homodyning.**

I. Introduction

THE increasing demand for high-throughput communication links drives the development of optical communication technologies. In recent years a massive growth in system throughput has been shown, mainly based on the channel scaling enabled by space division multiplexing (SDM) which exploits several cores and/or fiber modes to transmit independent data. In 2017, system throughput reached 10 Pb/s in a demonstration using >100 modes and extending over the C and L-band [1]. The total channel count exceeded 80 000, showing the massive scaling in systems employing broadband transmission and multiple modes. At the same time, >50 Tb/s throughput over >17 000 km transmission distance using single-mode fiber (SMF) was demonstrated [2]. Here the authors used wavelength-division multiplexing (WDM) of 295 separate channels.

Optical frequency combs, which have been investigated extensively for applications in spectroscopy, metrology and communications, have been proposed as a solution to reduce the large number of lasers needed in fully loaded system. The most prominent generation techniques are based on parametric mixing in micro-ring resonators [3], electro-optic (EO) modulation [4] and mode-locked lasers [5]. Kerr combs from integrated micro-ring resonators have been used as a multi-wavelength light source to realize WDM transmission with >50 Tb/s throughput over the full C+L-band [3]. Comb generation using EO modulation has been studied extensively [6], [7] and was used for data transmission in [4]. Parametric broadening of comb-lines originating from an EO-comb was investigated in [8] and, using optimized design of the nonlinear broadening stage, a spectral flat spectrum over >100 nm was achieved [9]. The high power per line of such a comb source was used in a record experiment where the authors achieved 2.15 Pb/s aggregated throughput using a 22-core fiber [10]. Transmission using mode-locked lasers have been extensively studied, for example in the context of data center applications [5], and recent improvements include the addition of a resonant feedback structure enabling improved line quality [11].

In any communication system, to maximize system throughput the available bandwidth (BW) has to be used in the most efficient manner. Higher-order modulation formats such as polarization multiplexed M-ary quadrature amplitude modulation (PM-MQAM), such as PM-128QAM and PM-256QAM, carrying 14 and 16 bits per symbol respectively, increase the channel throughput compared to classical systems using, e.g., PM quaternary phase shift keying which is limited to 4 bits per symbol. However, higher order modulation formats require a higher optical signal-to-noise ratio (OSNR) (and corresponding electrical signal-to-noise ratio, SNR) to achieve the same resulting bit error rate (BER) and are more sensitive to system impairments such as laser phase noise [12]. Moreover, the limited effective number of bits from the transceiver digital-to-analog and

Manuscript received October 23, 2017; revised December 8, 2017; accepted December 14, 2017. Date of publication December 24, 2017; date of current version March 1, 2018. This work was supported by the Swedish research council under Grant 2014-06138). *(Corresponding author: Mikael Mazur.)*

M. Mazur, J. Schröder, P. A. Andrekson, and M. Karlsson are with the Photonics Laboratory, Fibre Optic Communication Research Centre (FORCE), Department of Microtechnology and Nanoscience, Chalmers University of Technology, Gothenburg SE-412 96, Sweden (e-mail: mikael.mazur@chalmers.se; jochen.schroeder@chalmers.se; peter.andrekson@chalmers.se; magnus.karlsson@chalmers.se).

A. Lorences-Riesgo was with the Photonics Laboratory, Fiber Optic Communication Research Centre (FORCE), Department of Microtechnology and Nanoscience, Chalmers University of Technology, Gothenburg SE-412 96, Sweden. He is now with the IT-Instituto de Telecomunicações, Aveiro 3810-193, Portugal (e-mail: abellorences@av.it.pt).

Color versions of one or more of the figures in this paper are available online at http://ieeexplore.ieee.org.

Digital Object Identifier 10.1109/JLT.2017.2786750

analog-to-digital converters (DACs/ADCs) limits the achievable SNR in multi-level modulation format systems [13]. To enable transmission of higher-order modulation formats at higher baud rates, powerful digital signal processing (DSP) and forward error correction (FEC) schemes are employed [14]. With this, state-of-the-art transceivers are now capable of transmitting PM-1024QAM at a symbol-rate of 66 Gbaud [15] and a fully integrated InP-based 32QAM transceiver capable of working at symbol rates of up to 100 Gbaud was demonstrated in [16].

The possibility to use a single high-quality light source to generate multiple WDM carriers makes frequency combs attractive for scaling transceivers from single channels to multi-Tb/s superchannels. In its simplest form, the carriers from the frequency combs are used as transmitter and local oscillator (LO) light sources. Each wavelength channel is then treated independently using conventional intradyne DSP and the main benefit arises from reduction in laser count. However, the phase-locked nature of the carriers can be exploited for joint processing of several wavelength channels, and complexity reduction by sharing the DSP-based carrier recovery within a spectral superchannel has been demonstrated [17]. Furthermore, as shown in [18], two optical pilot tones are enough to fully characterize the transmitter comb and by recovering the two tones at the receiver side, a phase-locked receiver comb can be regenerated. This technique of comb regeneration for self-homodyne detection was demonstrated in an all-optical scheme with Brillouin amplification [19] and in a scheme with an electrical phase-locked loop for performance improvement [20].

Here we expand the concept introduced in [21] where we proposed and demonstrated the use of comb-based superchannels together with a single shared optical pilot tone for high spectral efficiency (SE) transmission. The single pilot is used to lock the transmitter and receiver comb seed lasers, which reduces carrier offsets. This reduction facilitates blind DSP-based signal recovery for each wavelength channel modulated with 24 Gbaud PM-128QAM. We demonstrate transmission of a 14.2 Tb/s 55 carrier superchannel transmission over a single span of 50 km standard single-mode fiber (SSMF). At a resulting SE of 10.3 bits/s/Hz, our demonstration shows the potential for frequency combs and optical pilot tones to enable superchannels with high spectral efficiency.

II. Challenges of Blind Carrier Recovery

The introduction of more powerful FEC allows system to operate at a lower received SNR, or equivalently higher pre-FEC BER, and still meet required BER tolerances after decoding. As we will show in this section, operation in this lower SNR regime makes blind DSP more challenging due to more frequent symbol errors in the received data.

A received symbol y_k corresponding to the transmitted complex symbol x_k can, in presence of additive white Gaussian noise (AWGN) and carrier offsets, be expressed as

$$y_k = x_k \exp\left(j\left(2\pi \Delta f_0 T_0 k + \phi_k\right)\right) + n_k, \tag{1}$$

assuming ideal matched filtering [22], [23]. Here k denotes the time index, Δf_0 any residual frequency offset (FO) arising from small differences between the transmitter and receiver laser frequencies, T_0 the symbol period, ϕ_k the laser phase noise (combined for both the transmitter and receiver laser) and n_k the AWGN. To avoid any penalty from carrier offsets (frequency and phase), DSP-based tracking is normally used to compensate for a non-zero Δf_0 and ϕ_k.

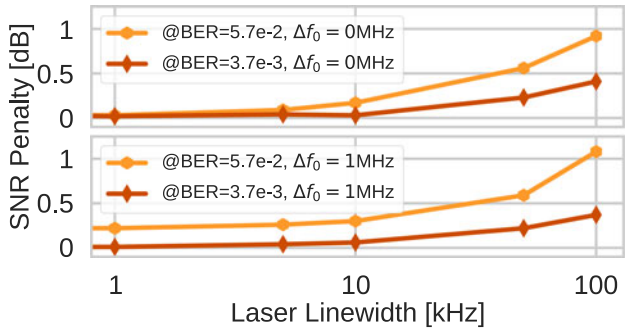

Fig. 1. Simulation results of SNR penalty from blind phase search for a 24 Gbaud 128QAM signal at two different target BERs, corresponding to a classical HD-FEC of $3.7 \cdot 10^{-3}$ and a modern SD-FEC limit of $5.7 \cdot 10^{-2}$. The required SNRs to achieve the target BER without any carrier offsets are 24 and 18 dB, respectively. The top figure corresponds to the case without any frequency offset, i.e., $\Delta f_0 = 0$ MHz, and the bottom figure to a residual frequency offset of $\Delta f_0 = 1$ MHz.

Complete carrier recovery is typically performed by first compensating FO in a coarse step and then tracking the phase noise and remaining FO. Several blind methods have been proposed to compensate for the FO [23]–[26]. One of the most commonly used algorithms for carrier phase estimation is blind phase search (BPS) which is a hardware compatible algorithm working for arbitrary modulation formats [12]. BPS uses a set of test angles and selects the angle resulting in the minimum distance between the received symbol and corresponding estimate of the transmitted symbol. To avoid errors due to additive noise [n_k in (1)], averaging over N symbols is used and the angle resulting in the minimum sum of all individual distances is selected.

The linewidth tolerance for BPS and modulation formats up to 256QAM has been studied using simulations, showing a required linewidth of 80 kHz for a 1 dB penalty at a BER of $1 \cdot 10^{-3}$ for a 10 Gbaud signal [12]. Since external-cavity lasers (ECLs) with a linewidth $<$100 kHz are now common, linewidth is not expected to result in a major degradation of system performance at $1 \cdot 10^{-3}$ target BER. However, modern systems are increasingly employing soft-decision (SD)-FEC instead of hard-decision (HD)-FEC. The pre-FEC BER operating target is therefore typically more than one order of magnitude higher, resulting in frequent symbol errors. The higher symbol-error count makes blind carrier recovery more challenging since a longer averaging filter is needed to suppress the noise at a lower SNR. This reduces the phase noise tolerance of the DSP, leading to more stringent requirements on laser linewidth.

The reduced tolerance is illustrated in Fig. 1(top) which shows the simulated receiver SNR penalty for a 24 Gbaud 128QAM signal as a function of laser linewidth. The simulation was based on (1) and the laser phase noise was simulated as a Wiener process, similar to [23]. We used BPS with 256 test-angles to

avoid any penalty due to limited angular resolution. The block size was swept in steps of 32 symbols to a maximum length of $N = 512$ and was optimized for each point. Every data point was calculated by averaging over 5 independent simulations of 2^{16} symbols each.

The selected operating points correspond to a classical HD-FEC with about 7% overhead (OH) [27] and a modern, powerful SD-FEC with 28% OH [14]. For 128QAM and AWGN only, the HD-FEC operating point corresponds to a SNR of 24.1 dB and the SD-FEC point to a lower SNR of 18.2 dB. We observe that for linewidths up to about 10 kHz the SNR penalty for the two operating points is very similar. As the linewidth increases beyond 50 kHz, the SNR penalty at the SD-FEC (lower SNR) operating point increases more rapidly due to the lower linewidth tolerance caused by the longer averaging filter needed to account for AWGN. Fig. 1(bottom) shows similar simulations but now including a FO of $\Delta f_0 = 1$ MHz. Compared to the previous case, we observe a penalty floor for operation in the lower SNR regime. The penalty is present even for low linewidths in contrast to the case of operating at the higher SNR. As the linewidth increases beyond 50 kHz we observe a growing penalty due to the combined effect of both FO and phase noise.

The tolerance to carrier offsets is significantly lower when working at a lower SNR. Therefore, linewidth and stability requirements strongly depend on the system operating conditions. Note that a residual FO of $\Delta f_0 = 1$ MHz might seem a high value, but for schemes such as [24] the accuracy depends on the number of symbols in the Fourier-transform implementation. In real-time systems this is typically limited to about 4096 symbols [28]. This results in estimation errors on the order of tenths of MHz and to ensure a residual sub-MHz FO requires the use of about 100000 symbols. The higher sensitivity to imperfections at the lower SNR operating point is not limited to FO, and any additional carrier offset or noise source causing a reduced SNR will degrade the tracking tolerance. For this reason, most demonstrations of higher-order QAM transmission have either used digital pilot symbols with up to 10% OH [29] or high-coherence lasers together with self-homodyne detection [30].

III. Comb-Based Superchannels Using a Single Optical Pilot Tone

The use of frequency combs as WDM source both in the transmitter and receiver raises new possibilities and challenges for carrier recovery. A standard comb-based transmission system uses independent combs at transmitter and receiver. Therefore, carrier offsets originating from differences between the comb seed lasers and additional FO from different line spacing and line-dependent phase noise could be present [31]. Thus, we extend (1) to

$$y_{m,k} = x_{m,k} \exp\left(j\left(2\pi\left(\Delta f_0 + m\Delta f_1\right) T_0 k + \phi_k + \varphi_{m,k}\right)\right) + n_{m,k}, \quad (2)$$

where Δf_1 denotes the difference in frequency spacing, $\varphi_{m,k}$ is the phase noise originating from the comb generation and m is the selected comb line index with $m = 0$ corresponding to the central line. Following (2), the combined impact from carrier offsets depends on the quality of the seed lasers as well as the comb generation. In the general case, the variance of the phase noise $\varphi_{m,k}$ on individual comb lines can increase with the line index m [17], [31], [32].

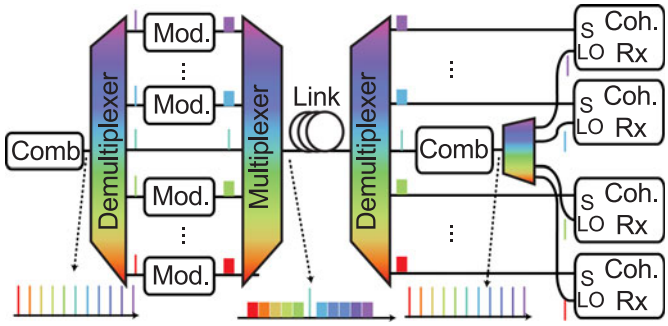

Fig. 2. Concept for the proposed comb-based superchannel transmission system using a single unmodulated optical pilot tone. The pilot tone is used to phase-lock the receiver comb seed laser to the transmitter comb. This reduces carrier offsets, which relaxes requirements on DSP-based carrier recovery while avoiding additional overhead and complexity normally associated with optical pilot tones.

Optical pilot tones can be used to overcome penalties due to FO and laser phase noise for individual channels [30]. An unmodulated copy of the transmitter laser is transmitted as a pilot tone to the receiver where the LO is phase-locked to the incoming tone. This cancels out the FO and, depending on the path-matching conditions and laser performance, the phase variations can be reduced by several orders of magnitude [33]. However, using a single tone for each wavelength channel results in a large SE loss and high transceiver complexity.

By using frequency combs, the advantage from optical pilot tones can be maintained while reducing both the complexity and loss in SE as conceptually illustrated in Fig. 2. The phase-locked nature of the carriers from a frequency comb implies that the carrier offsets from the seed laser are shared among all data channels within a comb-based superchannel. As a direct result of this, a single pilot tone can carry enough information from the transmitter to the receiver to enable cancellation of these offsets for all wavelength carriers. This is done by phase-locking the receiver comb seed laser to the incoming pilot tone which removes any laser frequency offset $\Delta f_0 = 0$ and suppresses the laser phase noise. As a result of this, (2) reduces to

$$y_{m,k} = x_{m,k} \exp\left(j\left(2\pi m \Delta f_1 T_0 k + \phi'_k + \varphi_{m,k}\right)\right) + n_{m,k}, \quad (3)$$

with ϕ'_k denoting the remaining laser phase noise. Similar to conventional pilot tones, the noise suppression shown in (3) depends on the path-matching conditions and laser performance. In addition, dispersion walk-off will contribute to a phase decorrelation within the superchannel [18], which will degrade the effective phase noise suppression from the optical pilot tone at long distances. However, the benefit of reducing frequency offsets will remain and as can be seen in Fig. 1, the fact that frequency offsets are reduced already translates into a penalty reduction. Equation (3) shows that, for high quality combs, carrier offsets can be reduced at the same complexity as for an equivalent single carrier system by locking the comb seed lasers. Only a single pilot tone is required for the transmission and recovery stage and all data channels share the improvement due to the

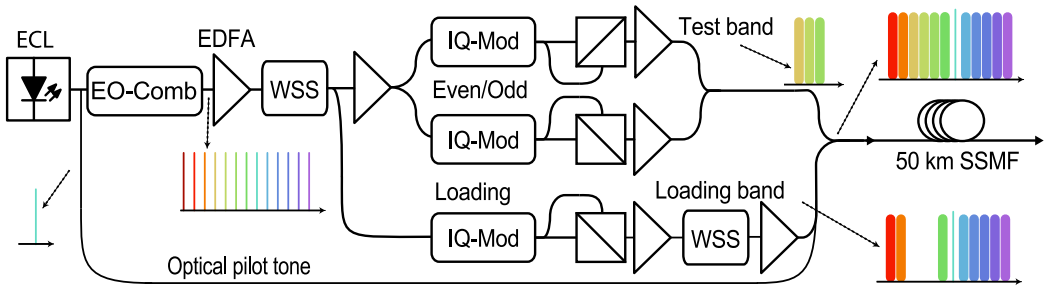

Fig. 3. Experimental setup for the superchannel transmitter using the test-loading band approach with a 5 channel wide testband. Each data channel was modulated using 24 Gbuad PM-128QAM and the pilot tone was extracted by tapping off light from the transmitter comb seed laser.

reduced carrier offset. The resulting requirements for the DSP-based carrier recovery are relaxed and only dictated by the comb properties instead of the seed lasers.

For systems using EO-combs, Δf_1 and $\varphi_{m,k}$ originates from differences between the radio frequency (RF)-clock used in each comb. Assuming high-quality clocks and combs seeded by standard ECLs, the carrier offsets originating from the ECLs are orders of magnitude larger compared to the offsets from the RF clocks, i.e., $\Delta f_1 \ll \Delta f_0$ and $\varphi_{m,k} \ll \phi_k, \forall m, k$. In our case, we measured an RF clock frequency difference $<$30 kHz over a time period of several days. Thus, the FO is below 1 MHz even for a 50 channel superchannel when locking the seed lasers. In contrast, the FO between combs using free-running ECLs is on the order of hundreds of MHz.

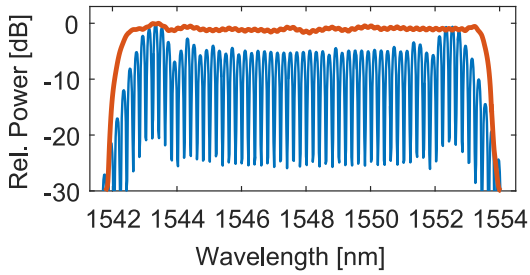

Fig. 4. Spectra of the transmitter frequency comb (blue, 0.1 nm resolution) and the resulting superchannel after combining the 54 data channels with the optical pilot tone (orange, 0.5 nm resolution). The frequency comb spacing was 25 GHz and all data channels were modulated using 24 Gbaud PM-128QAM.

IV. Experimental Setup

Here we present the experimental setup for evaluating the concept of sharing a single pilot tone within a comb-based superchannel shown in Fig. 2. We used an EO-comb generating about 55 lines with 25 GHz spacing as our superchannel light source. Out of these, 54 were modulated with 24 Gbaud PM-128QAM data and one was used as a pilot tone to enable injection-locking of the receiver comb seed laser to the transmitter comb.

A. Transmitter

The experimental setup for the transmitter is shown in Fig. 3. We used a standard ECL (100 kHz maximum specified linewidth) to seed our transmitter comb. The transmitter comb was built using two phase modulators followed by an intensity modulator to achieve a flat output spectrum, similarly to the comb described in [7]. All modulators were standard Lithium-Niobate modulators. The phase modulators had $V_\pi = 3.1$ V and the driving RF signal was amplified to 34 dBm resulting in about 26 generated comb lines per modulator. All modulators were driven by a common 25 GHz RF clock and the resulting output spectrum can be seen in Fig. 4. The total insertion loss for the EO-comb was about 15 dB and to maintain a high output OSNR the seed laser was amplified to an input power to the comb of about 27 dBm. The output of the EO-comb was amplified before a wavelength selective switch (WSS) was used to separate a 5 line testband from the remaining carriers and to suppress the center line corresponding to the pilot tone position. The testband was amplified and an optical interleaver (OI) was used to separate the lines into even and odd lines. These lines were then modulated independently using two separate IQ-modulators. Each modulator was driven using 2 independent DACs operating at 60 GS/s to modulate the 24 Gbaud 128QAM signal shaped with a root-raised cosine filter with a roll-off factor of 1%.

To compensate for any pattern-dependent distortions we used a 3 symbol memory look-up table approach [34]. The look-up table contained complex correction factors for each 3 symbol sequence $[x_{k-1}, x_k, x_{k+1}]$ of our transmitted pattern. To train it, we averaged over 10^6 received symbols and the look-up table correction corresponded to the average complex error $e_k = \mathbf{E}[y_k - x_k]$, where the expectation value operator $\mathbf{E}$ is calculated over all realizations of each unique 3-symbol sequence in the received data. The pattern was chosen by randomly generating bits and the total pattern length was 2^{16} symbols, being limited by the available memory in our arbitrary waveform generator. After modulation, polarization multiplexing was emulated using the split-delay-combine method with a delay of about 10 ns. To avoid additional OSNR degradation, the even and odd channels were first individually amplified before being recombined in a second OI.

The remaining channels (all channels not being part of the testband or corresponding to the pilot tone wavelength) were amplified and modulated using a third modulator to generate the loading channels. The loading modulator was driven with a time-delayed inverted copy of the pattern driving one of the testband modulators and polarization multiplexing was emulated similarly to the channels in the testband. The loading channels were then amplified and a second WSS was used to

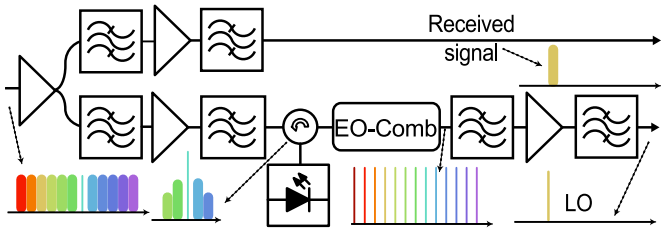

Fig. 5. Schematic of the superchannel receiver setup. Two paths were used in order to separate the data channels and the pilot tone. The pilot one was used to lock of the receiver comb to the transmitter comb, reducing carrier offsets and facilitating blind DSP-based carrier recovery.

suppress amplified spontaneous noise (ASE) on the location of the testband and the location of the pilot tone. The loading channels were amplified again and combined with the testchannels. The pilot was generated by tapping of 10% of the output light from the transmitter laser prior to amplification and was combined with the data channels to form the complete superchannel. The resulting spectrum can be seen in Fig. 4. The full superchannel was transmitted over a single-span of 50 km SSMF with a span loss of about 11 dB.

B. Receiver

The experimental setup for the proposed superchannel receiver is shown in Fig. 5. After initial amplification, the superchannel was separated into two arms to enable simultaneous utilization of the optical pilot tone and detection of the data channels. To filter out the pilot tone we used a 0.3 nm (3 dB BW and Gaussian filter shape) wide optical filter to suppress the neighboring data channels prior to injection locking of a standard distributed feedback laser with 18 dBm output power and a free-running linewidth of about 1 MHz. We found that an injection ratio of −40 dB (defined as the input over output slave laser power ratio) resulted in the best trade-off between long-term stability and filtering bandwidth. At this injection ratio we observed a filtering bandwidth on the order of several hundreds of MHz and locking stability over several hours. The bandwidth was sufficient to cover temporal drifts between the master and slave laser and residual performance fluctuations are mainly attributed to polarization drifts on the slave laser input signal, as further discussed in Section V-B. The slave laser output was then amplified and fed to the receiver EO-comb, built the same way as the transmitter comb and driven using a fully independent (no connection to the transmitter comb) RF-clock. The comb output was then amplified before selecting the proper LO line.

In the other arm, the corresponding data channel was filtered out using a 0.3 nm wide optical filter. To emulate a WDM de-multiplexer and ensure effective suppression of the neighboring channels, this filter was implemented using a third WSS. The selected data channel and LO line were then combined in a standard dual-polarization coherent optical receiver and the electrical outputs were sampled using a 50 GS/s real-time oscilloscope with 23 GHz analog BW. Offline DSP was implemented and consisted of initial front-end imbalance correction followed by resampling to 2 samples per symbol. In the case of single span transmission, a static dispersion compensation equalizer was used to remove chromatic dispersion. Polarization de-multiplexing and channel equalization was implemented using a dynamic equalizer with 45 $T_0/2$-spaced taps, updated using a decision-directed least mean square algorithm (DD-LMS). Phase tracking was implemented using the standard BPS algorithm, as discussed in Section II, using 64 test angles.

System performance was evaluated using both BER and generalized mutal information (GMI) [35]. We assumed a BER target of $5.7 \cdot 10^{-2}$ and accounted for a 28% OH for FEC, similar to the work in [36]. Implementations of such codes was studied in [14] based on spatially coupled low-density parity check codes. BER is the conventional, most commonly used, metric for evaluating system performance. With relationships between a given pre-FEC BER and a corresponding post-FEC BER after decoding existing given the use of HD decoding and assumptions on interleaving the coded bits, BER is suitable for estimating performance of such systems. Estimation of post-FEC BER from pre-FEC BER cannot be reliable done when assuming the use of SD-FEC [35]. When working with powerful SD-FEC codes, GMI has been shown to better estimate the post FEC performance compared to BER and with the assumption of 28% SD-FEC OH in this work, GMI calculation was necessary to verify system performance. The GMI for each channel corresponds to the highest achievable throughput using an optimal bit-wise SD-FEC with a memory-less receiver [35]. While practical implementations using finite length codes usually have a certain penalty with respect to the GMI, it is still a suitable estimator for system performance and design and implementations of corresponding codes are beyond the scope of this paper.

In this work we calculated the BER and GMI using about $2.5 \cdot 10^5$ symbols for each polarization, corresponding to about $1.8 \cdot 10^6$ bits. Adding to this, the BER is calculated using the received bits on both polarizations. The GMI was calculated by first estimating the received SNR and then calculate the corresponding L-values for a soft demapper [35, (29)]. The L-values were then used to estimate the GMI per transmitted bit [35, (30)] and the total GMI was found by summing this over all the 14 bits present in each 4D symbol.

V. Result

Here we present the results from the superchannel transmission experiment using the single shared optical pilot tone to reduce carrier offsets. Results from noise-loading experiments to evaluate the transmitter are shown first followed by back-to-back (B2B) evaluation of the superchannel. Finally, we present the results from the single span transmission experiment.

A. Noise Loading

To isolate any transceiver implementation penalty due to the use of PM-128QAM at a relatively high baudrate of 24 Gbaud, we first studied the performance of a single carrier in a B2B

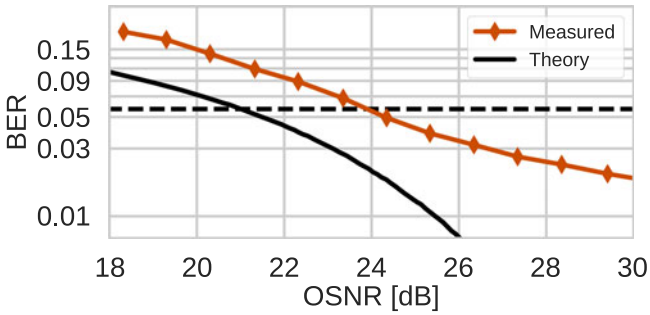

Fig. 6. BER as a function of optical signal to noise ratio (OSNR) for a single channel in back-to- configuration. The resulting implementation penalty at the target BER of $5.7 \cdot 10^{-2}$ (dotted line) was 3 dB.

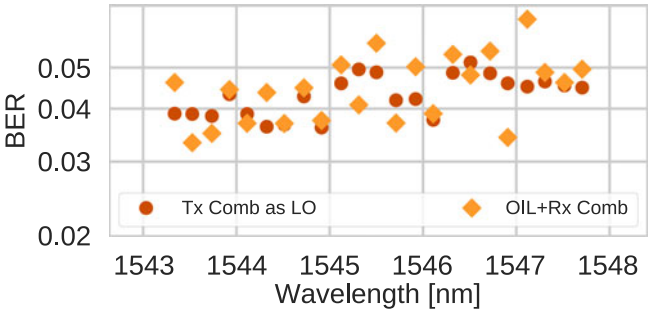

Fig. 7. Comparison between using the transmitter comb to generate the LO lines and the locked receiver comb. The slightly larger variation in BER when using the proposed injection-locked receiver compared to self-homodyne detection is due to instabilities in the locking process.

scenario. A variable optical attenuator was placed after the polarization-multiplexing emulation stage, in one of the arms in Fig. 3, and the output was connected directly to the receiver. The resulting BER as a function of OSNR is shown in Fig. 6. We observe a high error floor around a BER of $1 \cdot 10^{-2}$ which is due to transceiver impairments including the low effective number of bits (about 4.5) for 24 Gbaud signals. The corresponding implementation penalty at the target BER level of $5.7 \cdot 10^{-2}$ was about 3 dB.

B. Back-to-Back Characterization

We evaluated the performance of the proposed single optical pilot-tone scheme in comparison with the case of using the transmitter comb for generating both the data carriers and LO lines in a full B2B configuration. Due to the SNR being limited by transceiver noise, even in this case of B2B measurements, intradyne detection was not possible since large residual carrier offsets resulted in difficulties for our dynamic equalizer to converge as well as caused severe cycle slip events, resulting in unusable BER estimates.

The BER results for both cases tested on a subset of the lower wavelength channels (with respect to the pilot tone) are shown in Fig. 7. It is worth noticing here that out of the 5 data channels present in the test band we only measured the central 3 to ensure that each channel under test had two high-OSNR neighboring channels. In Fig. 7 when the same comb was used for transmission and LO, we can observe a grouping of the BERs in groups of 3 caused by our measurement method.

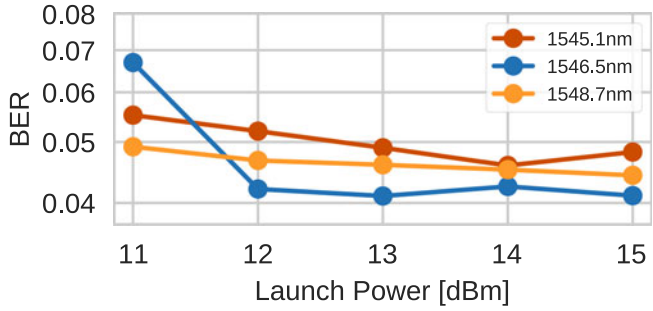

Fig. 8. Resulting BER as a function of total superchannel launch power for 3 wavelength channels. A total launch power of 14 dBm was found to result in the best overall performance.

The difference between individual test band can be attributed to a number of transceiver imperfections, including variations in flattening performance since re-flattening was required when shifting the testband position.

When using the pilot-tone based receiver we observe a slightly larger variation in BER. This variation was mainly due to differences in slave-laser performance which can be attributed to two main contributions. First, difference in the achieved transmitter flattening affected the suppression of noise on the pilot tone wavelength. More importantly, injection locking is a polarization-sensitive process and polarization drifts caused variations in slave laser input power. Measuring the channels in Fig. 7 was done using automated serial measurements that lasted for several hours at the time without active tracking of the slave-laser input. To overcome this issue, active polarization tracking or the use of a more complex polarization-insensitive injection locking scheme [37] should be implemented.

C. 50 km Transmission

To further evaluate performance of the proposed scheme we performed transmission over one span of 50 km SSMF. We first optimized the transmitted power by performing a launch power sweep and the resulting BERs for launch powers ranging from 11 to 15 dBm for three selected channels are plotted in Fig. 8. We found that a total launch power of 14 dBm, corresponding to about -3 dBm per channel, resulted in the lowest overall BER. The pilot tone launch power was equal to the same as the data channels.

BER and GMI measurements for all the 54 wavelength channels after transmission are shown in Fig. 9. The min, mean and max of the measured BERs for each channel were $3.4 \cdot 10^{-2}$, $4.4 \cdot 10^{-2}$ and $5.3 \cdot 10^{-2}$, respectively. These values are below the $5.7 \cdot 10^{-2}$ FEC threshold assuming 28% coding OH [36]. The total superchannel throughput was 14.2 Tb/s with a resulting SE of 10.3 bits/s/Hz, accounting for the FEC OH, the guardband between the carriers and the optical pilot tone. In terms of GMI, the corresponding minimum, mean and maximum values were 11.3, 11.8 and 12.3 bits/s/Hz respectively. We note that the corresponding assumption of 28% FEC OH corresponds to a theoretical minimum required GMI of 10.9 bits/s/Hz which leaves margin for a practical FEC implementation. Based on the GMI, we also calculated an achievable information rate AIR_{WDM} [38] which takes into account the coding OH as well

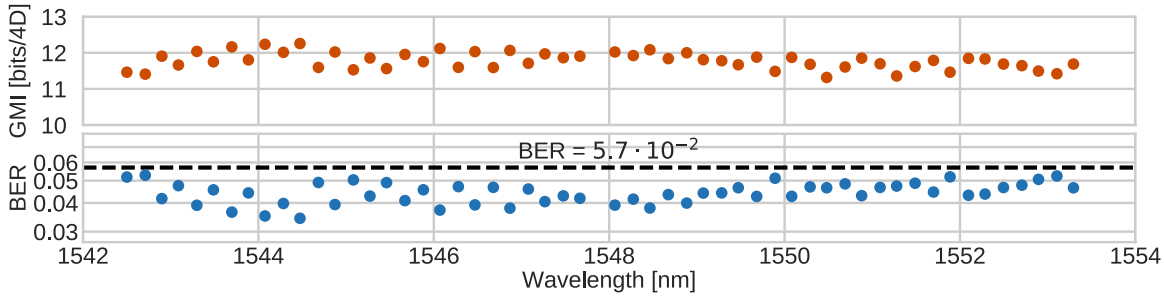

Fig. 9. Resulting BER and GMI values for all 54 data channels within the spectral superchannel. All measured BERs were below the assumed threshold of $5.7 \cdot 10^{-2}$ corresponding to a SD-FEC overhead of 28%.

as the OH for transmitting the pilot tone and the guard-band between the channels. The corresponding AIR_{WDM} for our superchannel was 11.1 bits/s/Hz, and the corresponding throughput, assuming optimized coding for each individual wavelength channel, was 15.3 Tb/s.

VI. Discussion

Optical pilot tones offer a significant reduction in carrier offset that can be of great importance for higher-order modulation transmission using conventional ECLs with linewidths around 100 kHz and blind DSP-based carrier recovery. However, the increased data throughput achieved through moving to high modulation orders has to outweigh the SE loss due to the transmission of the pilot and the complexity increase, in particular compared to the alternative of transmitting digital pilot symbols.

The demonstrated scheme of transmitting a single optical pilot tone inside a spectral superchannel is a good compromise between added complexity, pilot OH and performance. In contrast to full phase-locking of the receiver comb to the transmitter which requires two pilot tones [19], [20], the SE loss is reduced by half. Similarly the complexity of the receiver is significantly reduced as only a single injection locking stage and no phase-locked loops are required. The overhead and complexity can further be reduced by making use of the spatial domain in systems employing SDM to increase system throughput. For networks having several nodes employing frequency combs, optical pilot tones can be used to lock all comb sources to a seed source, reducing the overall DSP complexity while maintaining low pilot overhead [39].

Another technique to reduce OH of optical pilot tone systems at the expense of additional complexity was investigated in, e.g., [30] for single-carrier transmission and in [40] for WDM transmission. The authors used a scheme of frequency up-shifting the pilot tones out of the data channel band. In superchannel transmission a gap between subchannels is required, reducing the SE. More importantly each subchannel requires a complex injection locking and frequency shifting setup. Compared to our method, where OH scales as 1/N (where N is the subchannel count) and only a single injection locking setup, the scheme is advantageous when transmitting independent WDM channels or superchannels with relatively few subchannels. However, under those conditions, the added complexity needs to be compared against transmitting digital pilot symbols with comparable OH at equivalent modulation formats [36].

Superchannels have the potential of leveraging on strong benefits from integration and full co-integration of two high-baudrate transceivers on a single chip has been demonstrated [41]. For systems like the one proposed in this work, a single comb source on a chip is needed. Candidates for comb sources on a chip are multiple: including microring resonators [3], EO-combs [42] and quantum-dash mode-locked lasers [11]. The potential for joint co-integration of both frequency combs and OIL was furthermore demonstrated in [43] where the authors used OIL to filter out and ensure equal line power of the comb lines for modulation.

In addition, the injection locking stage could be replaced by any other filtering technique with low BW, which avoids degradation of the LO carriers due the received OSNR on the pilot tone. If the receiver used a microring resonator as comb source, the resonator could also be used as a filter for the incoming pilot tone [44]. In such a case, the addition of a drop-port to the comb-generating microring could be used to avoid penalty from ASE transferred from the pilot tone [45].

VII. Conclusion

We have shown how the phase-locked nature of carriers from frequency combs enables effective sharing of a single optical pilot tone within spectral superchannels. By phase-locking the receiver frequency comb to the pilot tone, carrier offsets are reduced. This facilitates the use of blind DSP-based carrier recovery together with higher-order modulation formats at relative low receiver SNRs. The proposed scheme has experimentally been demonstrated by transmission of a comb-based 54 × 24 Gbaud PM-128QAM superchannel using standard blind DSP. The shared scheme limited the pilot tone overhead to <2%, resulting in a spectral efficiency of 10.3 bits/s/Hz after 50 km SSMF transmission with EDFA-only amplification. This demonstrates the potential for optical pilot tones to enable comb-based superchannels with high spectral efficiency.

References

[1] D. Soma *et al.*, "10.16 Peta-bit/s dense SDM/WDM transmission over low-DMD 6-mode 19-core fibre across C+L band," in *Proc. Eur. Conf. Opt. Commun.*, 2017, Paper Th.PDP.A.1.

[2] J.-X. Cai *et al.*, "51.5 Tb/s capacity over 17,107 km in C+L bandwidth using single mode fibers and nonlinearity compensation," in *Proc. Eur. Conf. Opt. Commun.*, 2017, Paper Th.PDP.A.2.

[3] P. Marin-Palomo *et al.*, "Microresonator-based solitons for massively parallel coherent optical communications," *Nature*, vol. 546, no. 7657, pp. 274–279, 2017.

[4] W. Mao, P. A. Andrekson, and J. Toulouse, "Investigation of a spectrally flat multi-wavelength DWDM source based on optical phase- and intensity-modulation," in *Proc. Opt. Fiber Commun. Conf.*, 2004, Paper MF78.

[5] V. Vujicic *et al.*, "Quantum dash mode-locked lasers for data centre applications," *J. Sel. Topics Quantum Electron.*, vol. 21, no. 6, pp. 53–60, 2015.

[6] M. Fujiwara, J. Kani, H. Suzuki, K. Araya, and M. Teshima, "Flattened optical multicarrier generation of 12.5 GHz spaced 256 channels based on sinusoidal amplitude and phase hybrid modulation," *Electron. Lett.*, vol. 37, no. 15, pp. 967–968, 2001.

[7] A. J. Metcalf, V. Torres-Company, D. E. Leaird, and A. M. Weiner, "High-power broadly tunable electrooptic frequency comb generator," *J. Sel. Topics Quantum Electron.*, vol. 19, no. 6, pp. 231–236, 2013.

[8] R. Slavik *et al.*, "Stable and efficient generation of high repetition rate (>160 GHz) subpicosecond optical pulses," *IEEE Photon. Technol. Lett.*, vol. 23, no. 9, pp. 540–542, May 2011.

[9] V. Ataie, E. Myslivets, B. P.-P. Kuo, N. Alic, and S. Radic, "Spectrally equalized frequency comb generation in multistage parametric mixer with nonlinear pulse shaping," *J. Lightw. Technol.*, vol. 32, no. 4, pp. 840–846, Feb. 2014.

[10] B. Puttnam *et al.*, "2.15 Pb/s transmission using a 22 core homogeneous single-mode multi-core fiber and wideband optical comb," in *Proc. Eur. Conf. Opt. Commun.*, 2015, Paper PDP3.1.

[11] J. N. Kemal *et al.*, "32QAM WDM transmission using a quantum-dash passively mode-locked laser with resonant feedback," in *Proc. Opt. Fiber Commun. Conf.*, 2017, Paper Th5C.3.

[12] T. Pfau, S. Hoffmann, and R. Noé, "Hardware-efficient coherent digital receiver concept with feedforward carrier recovery for M-QAM constellations," *J. Lightw. Technol.*, vol. 27, no. 8, pp. 989–999, Apr. 2009.

[13] R. H. Walden, "Performance trends for analog to digital converters," *IEEE Commun. Mag.*, vol. 37, no. 2, pp. 96–101, Feb. 1999.

[14] F. Buchali, A. Klekamp, L. Schmalen, and D. Tomislav, "Implementation of 64QAM at 42.66 GBaud using 1.5 samples per symbol DAC and demonstration of up to 300 km fiber transmission," in *Proc. Opt. Fiber Commun. Conf.*, 2014, Paper M2A.1.

[15] R. Maher, K. Croussore, M. Lauermann, R. Going, X. Xu, and J. Rahn, "Constellation shaped 66 GBd DP-1024QAM transceiver with 400 km transmission over standard SMF," in *Proc. Eur. Conf. Opt. Commun.*, 2017, Paper Th.PDP.B.2.

[16] V. Lal *et al.*, "Extended C-band tunable multi-channel InP-based coherent transmitter PICs," *J. Lightw. Technol.*, vol. 35, no. 7, pp. 1320–1327, Apr. 2017.

[17] L. Lundberg, M. Mazur, A. Lorences-Riesgo, M. Karlsson, and P. A. Andrekson, "Joint carrier recovery for DSP complexity reduction in frequency comb-based superchannel transceivers," in *Proc. Eur. Conf. Opt. Commun.*, 2017, Paper Th.1.D.3.

[18] A. Lorences-Riesgo, T. A. Eriksson, A. Fülöp, P. A. Andrekson, and M. Karlsson, "Frequency-comb regeneration for self-homodyne superchannels," *J. Lightw. Technol.*, vol. 34, no. 8, pp. 1800–1806, Apr. 2016.

[19] A. Lorences-Riesgo, M. Mazur, T. A. Eriksson, P. A. Andrekson, and M. Karlsson, "Self-homodyne 24 x 32-QAM superchannel receiver enabled by all-optical comb regeneration using Brillouin amplification," *Opt. Express*, vol. 24, no. 26, pp. 29 714–29 723, 2016.

[20] M. Mazur, A. Lorences-Riesgo, M. Karlsson, and P. A. Andrekson, "10 Tb/s self-homodyne 64-QAM superchannel transmission with 4% spectral overhead," in *Proc. Opt. Fiber Commun. Conf.*, 2017, Paper Th3F.4.

[21] M. Mazur, A. Lorences-Riesgo, J. Schröder, P. A. Andrekson, and M. Karlsson, "10.3 bits/s/Hz spectral efficiency 54× 24GBaud PM-128QAM comb-based superchannel transmission using single pilot," in *Proc. Eur. Conf. Opt. Commun.*, 2017, Paper M.2.F.4.

[22] D. Huang, T.-H. Cheng, and C. Yu, "Accurate two-stage frequency offset estimation for coherent optical systems," *IEEE Photon. Technol. Lett.*, vol. 25, no. 2, pp. 179–182, Jan. 2013.

[23] E. Ip and J. M. Kahn, "Feedforward carrier recovery for coherent optical communications," *J. Lightw. Technol.*, vol. 25, no. 9, pp. 2675–2692, Sep. 2007.

[24] M. Selmi, Y. Jaouen, and P. Ciblat, "Accurate digital frequency offset estimator for coherent PolMux QAM transmission systems," in *Proc. Eur. Conf. Opt. Commun.*, 2009, Paper P3.08.

[25] A. Meiyappan, P. Y. Kam, and H. Kim, "On decision aided carrier phase and frequency offset estimation in coherent optical receivers," *J. Lightw. Technol.*, vol. 31, no. 13, pp. 2055–2069, Jul. 2013.

[26] D. Huang, T. H. Cheng, and C. Yu, "Accurate two-stage frequency offset estimation for coherent optical systems," *IEEE Photon. Technol. Lett.*, vol. 25, no. 2, pp. 179–182, Jan. 2013.

[27] D. Qian *et al.*, "101.7-Tb/s (370 × 294-Gb/s) PDM-128QAM-OFDM transmission over 3 × 55-km SSMF using pilot-based phase noise mitigation," in *Proc. Opt. Fiber Commun. Conf.*, 2011, Paper PDPB5.

[28] D. A. Morero, M. A. Castrillón, A. Aguirre, M. R. Hueda, and O. E. Agazzi, "Design tradeoffs and challenges in practical coherent optical transceiver implementations," *J. Lightw. Technol.*, vol. 34, no. 1, pp. 121–136, Jan. 2016.

[29] H. Hu *et al.*, "Adaptive rates of high-spectral-efficiency WDM/SDM channels using PDM-1024-QAM probabilistic shaping," in *Proc. Eur. Conf. Opt. Commun.*, 2017, Paper Tu.1.D.1.

[30] S. Beppu, K. Kasai, M. Yoshida, and M. Nakazawa, "2048 QAM (66 Gbit/s) single-carrier coherent optical transmission over 150 km with a potential SE of 15.3 bit/s/Hz," *Opt. Express*, vol. 23, no. 4, pp. 4960–4969, 2015.

[31] A. Ishizawa *et al.*, "Phase-noise characteristics of a 25-GHz-spaced optical frequency comb based on a phase- and intensity-modulated laser," *Opt. Express*, vol. 21, no. 24, pp. 29 186–29 194, 2013.

[32] Z. Tong, A. O. J. Wiberg, E. Myslivets, B. P. P. Kuo, N. Alic, and S. Radic, "Spectral linewidth preservation in parametric frequency combs seeded by dual pumps," *Opt. Express*, vol. 20, no. 16, pp. 17 610–17 619, 2012.

[33] Y. Wang, K. Kasai, M. Yoshida, and M. Nakazawa, "Single-Carrier 216 Gbit/s, 12 Gsymbol/s 512 QAM coherent transmission over 160 km with injection-locked homodyne detection," 2017, Paper Tu2E.1.

[34] J. H. Ke, Y. Gao, and J. C. Cartledge, "400 gbit/s single-carrier and 1 tbit/s three-carrier superchannel signals using dual polarization 16-qam with look-up table correction and optical pulse shaping," *Opt. Express*, vol. 22, no. 1, pp. 71–84, 2014.

[35] A. Alvarado, E. Agrell, D. Lavery, R. Maher, and P. Bayvel, "Replacing the soft-decision FEC limit paradigm in the design of optical communication systems," *J. Lightw. Technol.*, vol. 34, no. 2, pp. 707–721, Oct. 2016.

[36] T. Rahman *et al.*, "Long-haul transmission of PM-16QAM, PM-32QAM and PM-64QAM based terabit superchannels over a field deployed legacy fiber," *J. Lightw. Technol.*, vol. 34, no. 13, pp. 3071–3079, Jul. 2016.

[37] J. Jignesh, B. Corcoran, J. Schröder, and A. Lowery, "Polarization independent optical injection locking for carrier recovery in optical communication systems," *Opt. Express*, vol. 25, no. 18, pp. 21 216–21 228, 2017.

[38] S. Chandrasekhar *et al.*, "High-spectral-efficiency transmission of PDM 256-QAM with parallel probabilistic shaping at record rate-reach tradeoffs," in *Proc. Eur. Conf. Opt. Commun.*, 2016, Paper Th.3.C.1.

[39] J. Sakaguchi, W. Klaus, B. Puttnam, J. M. D. Mendinueta, Y. Awaji, and N. Wada, "Spectrally-Efficient seed-lightwave-distribution system using space-division-multiplexed distribution channel for multi-core 3-mode-multiplexed DP-64QAM transmission," in *Proc. Eur. Conf. Opt. Commun.*, 2017, Paper M.1.E.1.

[40] T. Kan, K. Kasai, M. Yoshida, and M. Nakazawa, "42.3 Tbit/s, 18 Gbaud 64 QAM WDM coherent transmission over 160 km in the C-band using an injection-locked homodyne receiver with a spectral efficiency of 9 bit/s/Hz," *Opt. Express*, vol. 25, no. 19, pp. 22 726–22 737, 2017.

[41] R. Going *et al.*, "Multi-channel InP-based coherent PICs with hybrid integrated SiGe electronics operating up to 100GBd, 32QAM," in *Proc. Eur. Conf. Opt. Commun.*, 2017, Paper Th.PDP.C.3.

[42] R. Slavík, S. G. Farwell, M. J. Wale, and D. J. Richardson, "Compact optical comb generator using InP tunable laser and push-pull modulator," *IEEE Photon. Technol. Lett.*, vol. 27, no. 2, pp. 217–220, Jan. 2015.

[43] Z. Liu, S. Farwell, M. Wale, D. J. Richardson, and R. Slavik, "InP-based optical comb-locked tunable transmitter," in *Proc. Opt. Fiber Commun. Conf.*, 2016, Paper Tu2K.2.

[44] W. Bogaerts *et al.*, "Silicon microring resonators," *Laser Photon. Rev.*, vol. 6, no. 1, pp. 47–73, 2012.

[45] P.-H. Wang *et al.*, "Drop-port study of microresonator frequency combs: power transfer, spectra and time-domain characterization," *Opt. Express*, vol. 21, no. 19, pp. 22 441–22 452, 2013.

Authors' biographies not available at the time of publication.